(Online) ISSN 2712-0562
Original Research
Sustainable Engineering and Innovation
Vol. 7, No. 2, 2025, pp.355-364
https://doi.org/10.37868/sei.v7i2.id486

Wavelet decomposition and statistical characterization for unbalance detection in rotating systems

C. L. Sandoval-Rodriguez[1-2*], A. F. Jiménez-Quezada[2], C. G. Cárdenas-Arias[2-3], A. D. Rincón-Quintero[2-3], Humberto J. Navarro[1-2] and O. Lengerke[4]

[1] Research group on energy systems, automation and control - GISEAC, Unidades Tecnológicas de Santander, Bucaramanga, Colombia
[2] Faculty of Natural Sciences and Engineering, Unidades Tecnológicas de Santander, Bucaramanga, Colombia
[3] Research Group on Design and Materials – DIMAT, Unidades Tecnológicas de Santander, Bucaramanga, Colombia
[4] Advanced Control Research Group-GICAV, Unidades Tecnológicas de Santander, Bucaramanga, Colombia

*Corresponding author E-mail: csandoval@correo.uts.edu.co

Received Mar. 25, 2025
Revised Jun. 27, 2025
Accepted Jul. 7, 2025
Online Aug. 4, 2025

Abstract

Vibration analysis is a crucial tool for the early detection of faults in rotating machines, as it allows for the prevention of major damage and avoids significant costs associated with these faults. This study examines the phenomenon of imbalance in rotating machines, using signals generated on a test bench at the Santander Technological Units, where specific fault conditions were replicated. The signals obtained were analyzed using wavelet decomposition, from which key characteristics were extracted, such as root mean square (RMS), peak value, kurtosis, and mean absolute value (MAV). These characteristics were then compared using box plots to evaluate the separation between signals from unbalanced machines and those in a fault-free state. This analysis allowed us to identify significant differences between the two conditions, demonstrating the effectiveness of the approach in detecting faults due to imbalance.

Keywords: Wavelet, Vibration analysis, Predictive maintenance, Rotating machinery, Unbalance

1. Introduction

In the era of Industry 4.0, industrial predictive maintenance has a wide range of tools for early failure diagnosis and damage prevention. These tools include vibration analysis, ultrasound, thermography, and lubricant analysis, among others. In addition, these techniques are often combined with advanced technologies such as artificial intelligence (AI) and the Internet of Things (IoT) [1][2].

In the industrial sector, rotating machines have a defined period of useful life [3][4]. To monitor their condition over time, various indicators are used, such as failure probability density, cumulative probability of failure, and failure rate. These concepts are summarized in the well-known failure curve, also called the bathtub curve, which describes three stages: infant mortality, asset life, and wear and tear or aging [5]. For maintenance personnel, extending the service life of equipment is a priority [6]. According to the bathtub curve, the second

interval-the service life stage-is crucial, as it is during this period that machines often experience random failures. To mitigate these problems and avoid unnecessary costs, vibration analysis, a predictive maintenance technique that uses sensors to detect faults such as misalignment and unbalance, is used [7-10].

Unbalance occurs when the rotating mass is not uniformly distributed with respect to the axis of rotation, which generates centrifugal forces that destabilize the machine [11], [12], [13]. This phenomenon can be classified into two main types. Static unbalance, which occurs when the weight is not uniformly distributed in a single plane perpendicular to the axis of rotation. Dynamic unbalance, a more complex condition involving multiple planes of unbalance. Vibration analysis allows these faults to be identified and corrected before they cause significant damage to the machine [14], [15].

In this work, signals from a test bench with a rotating machine subjected to unbalanced conditions will be analyzed. From these signals, samples were taken at different frequencies, and the wavelet transform [16], [17] was applied for processing. Subsequently, features such as RMS and peak value of the decompositions were extracted and compared using box plots. The analyses included two configurations: one that considered all sensors together and one that separated the sensors on the X and Y axes. The best results were obtained when looking at the separation between unbalanced and fault-free signals [18].

2. Materials and methods

2.1. Vibration test bench

For this paper, a vibration bench (Figure 1), designed to simulate imbalance-related failures in rotating machinery, was used. The bench consists of a 3340 RPM, 1/2 HP WEG motor, two flywheels to induce imbalance, a flexible coupling, and a bearing-mounted shaft. Instrumentation included three 3300 XL 8mm proximity sensors connected to proximity transducers of the same model, compatible with a National Instruments NI-6008 data acquisition card controlled by LabVIEW software. The 3300 XL 8mm proximity sensors operate on the eddy current principle, enabling non-contact measurement of the dynamic displacement between the sensor and a rotating shaft. This model offers a sensitivity of 7.87 mV/μm (200 mV/mil) and a typical linear range of 0 to 2 mm, with excellent resolution (<1 μm) and a frequency response of up to 10 kHz, making it ideal for the precise monitoring of vibrations in rotating machinery. Its stainless-steel construction and reverse-mount configuration allow for robust and reliable integration, complying with the recommendations of the ISO 7919 standard for sensor placement and orientation on rotating machinery. The sensors were connected via a specially modified junction box, which incorporated male plugs and cable glands for proper organization and protection of the wiring. Each sensor was linked to its corresponding Proximitor, which delivers a voltage signal proportional to the detected displacement. These signals were directed to the differential analog inputs of the NI-6008 card, configured with a range of ±20V and a sampling frequency of 1 kHz. This configuration ensures reproducible and accurate conditions for evaluating the dynamic behavior of the shaft under controlled imbalance conditions.

Figure 1. Vibration test bench

2.2. Signal processing and features

Wavelet transform: The wavelet transform was used to decompose the signals acquired from the test bench, applying a fourth-order decomposition. The general equation is defined as follows [16], [17]:

$$W_f(s,\tau) = \int f(t)\Psi^*{}_{s,\tau}(t)\, dt \qquad (1)$$

Root mean square (RMS): we use it to calculate the mean value of our signal from the wavelet decomposition [19], [20], it is expressed in the following Equation 2:

$$RMS = \sqrt{\frac{1}{N}\sum_{i=1}^{N} X_i} \qquad (2)$$

Peak value: maximum value of the signal, as shown in Equation 3:

$$Peak = \max(X_i) \qquad (3)$$

Kurtosis is a statistical measure that describes the "shape" of a signal's probability distribution. Specifically, it indicates the concentration of data around the mean and the presence of heavy tails or outliers [21]. Where the mean is μ and the standard deviation is σ, kurtosis is calculated as:

$$\text{Kurtosis} = \frac{1}{N}\sum_{n=1}^{N}\left(\frac{x_i-\mu}{\sigma}\right)^4 \qquad (4)$$

Mean Absolute Value (MAV): It is a time-domain feature that calculates the average of the absolute values of the points in a signal.

$$MAV = \frac{1}{N}\sum_{n=1}^{N}|x_i| \qquad (5)$$

2.3. Statistical analysis

For the statistical analysis, box plots were used as a key tool to visualize the variance and separation between the different data sets obtained. These plots allow clear identification of the distributions of values, the presence of outliers, and significant differences between groups [22].

Additionally, bar graphs were generated in order to represent the values derived from the analyzed characteristics (such as RMS and peak value) for each sensor individually. This visualization allowed separating the sensor data on the X and Y axes; with these decompositions, the RMS, peak, MAV, and kurtosis values were calculated for each of the signals.

3. Results and discussion

The samples were taken by generating an imbalance on the test bench. Two sensors, referred to as X and Y for this test, were used at 45° from the vertical axis and 90° between them, as indicated by the ISO-7919 standard and the reference sensor. The data obtained by imbalance, free, and reference are available. For this data, programming was carried out in MATLAB to obtain the fourth-order wavelet decomposition, see Figure 2. With these decompositions, the RMS value, peak absolute mean value, and kurtosis were calculated for each of the signals.

RMS and Peak values were obtained for the following decompositions:

1. For the whole signal or vector of the wavelet decomposition.
2. The last decomposition or last approximation called cA3
3. And to the decompositions before the last detail (without cA3)

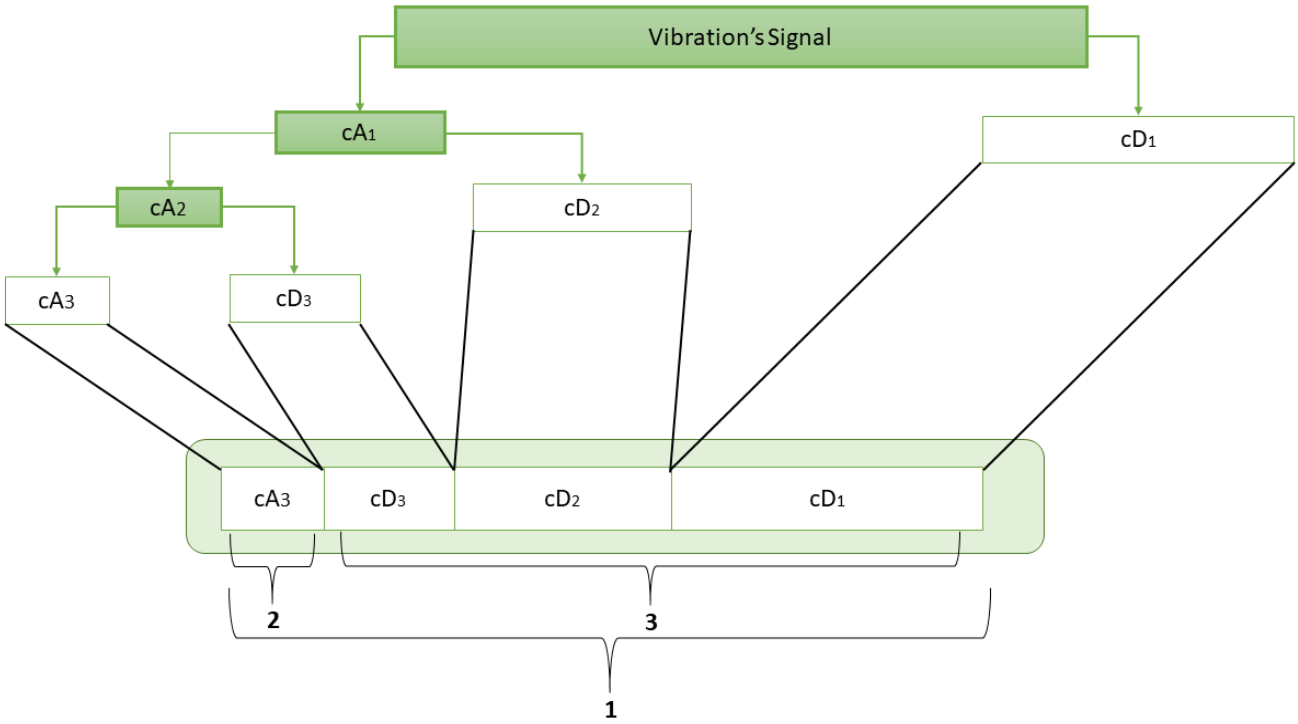

Figure 2. Wavelet decomposition

The RMS, Peak, MAV, and kurtosis values were used to compare the characteristics, as shown in Figure 2. The purpose of this comparison is to see the separation between unbalanced and free data, as the rotating machine should normally work. We can see that the RMS boxes with imbalance and RMS free tend to separate, but the total box does not, as does the kurtosis characteristic. When comparing the peak and MAV values, we observe that the values are relatively equal between the two boxes or averages. Table 1 shows in more detail the average for the peak value with an imbalance of 35. 1446 and a free peak of 34.8751.

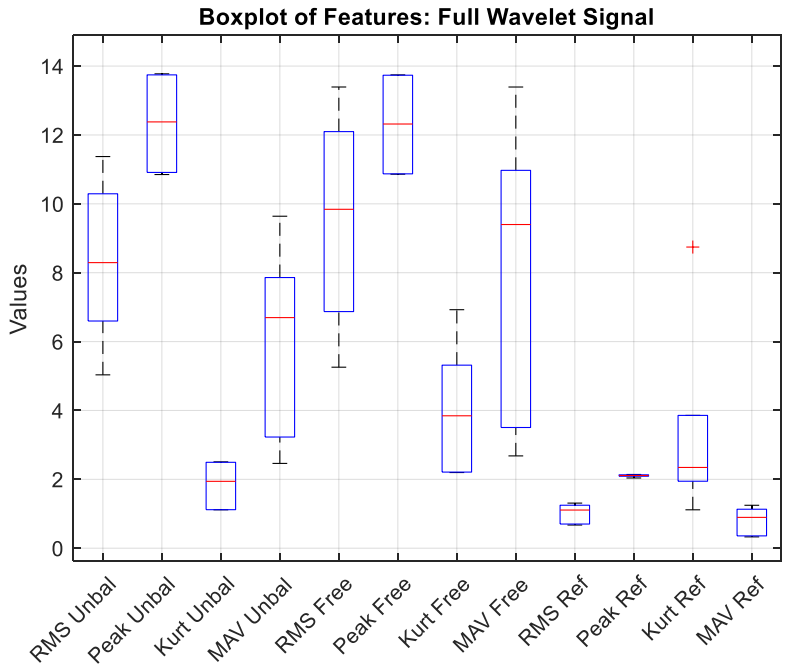

Figure 3. Boxplot signal or vector of the wavelet

In Figure 4, we see the boxplot for the data from the last cA3 decomposition. We see that the RMS and kurtosis characteristics have separated means, but the distribution of each box is wider for the 25th and 75th percentile

values, and the peak values are similar for the unbalanced and free data (Table 1). In Figure 5, we see the values of the characteristics for the rest of the decomposition (detail) without the last detail of the wavelet (cA3), but these values are very small. In Table 1, we see that there is not much difference in the values of the characteristics, so in Figure 6, we see the values of the characteristics for the rest of the decomposition (detail) without the last detail of the wavelet (cA3), but these values are very small. In Table 1, we see that there is not much difference in the values of the characteristics, so in Figure 6, we see the values decomposition (detail) without the last detail of the wavelet (cA3), but these values are very small. In Table 1, we see that there is not much difference in the values of the characteristics, which is why we say that the values are intertwined. Upon observing this, it is decided to continue working only with the RMS values of the entire decomposition and the data from the last detail cA3, values from Figures 3 and 4, respectively.

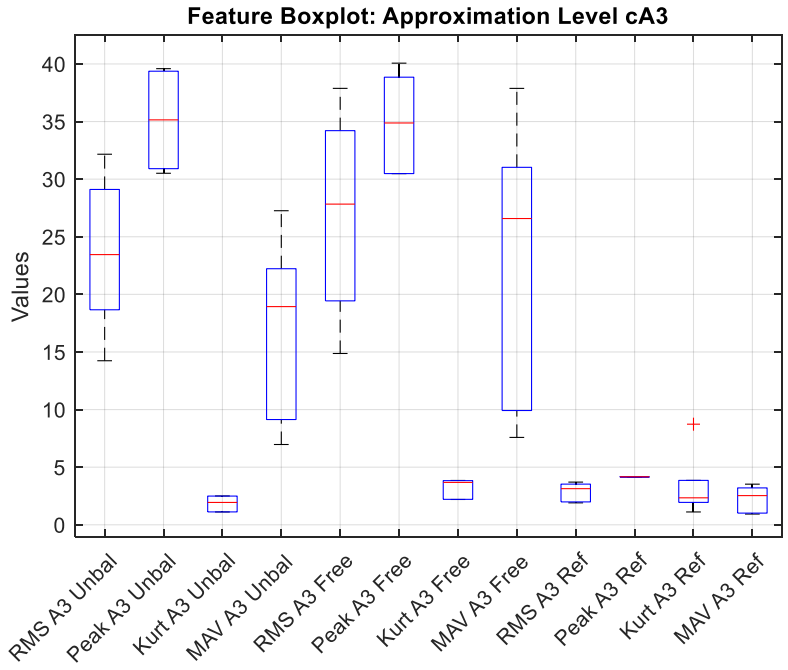

Figure 4. Boxplot decomposition or the last approximation called cA3

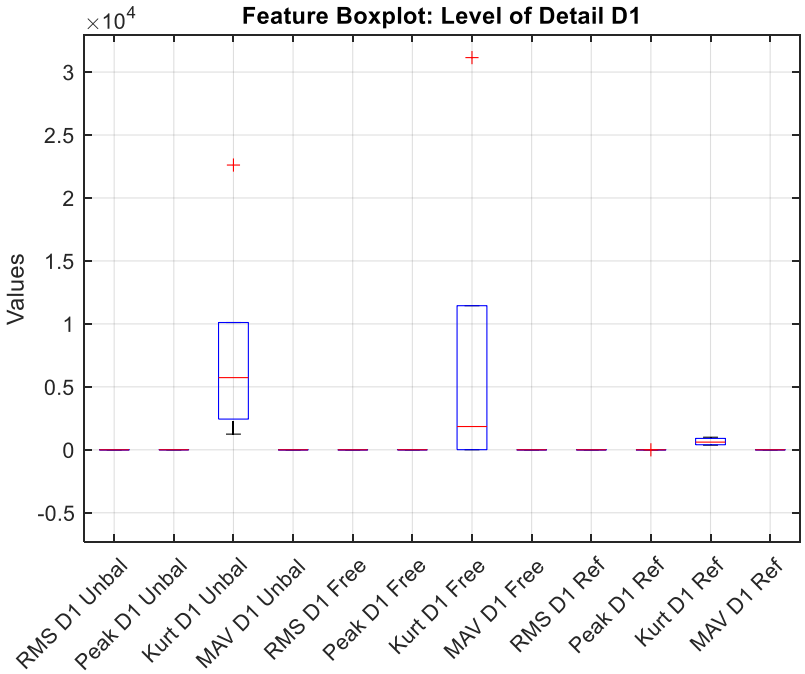

Figure 5. Boxplot decompositions before the last detail

Table 1. Median and IQR

	All decomposition		cA3	
Features	Median	IQR	Median	IQR
RMS unbalanced	8.2929	(6.5994,10.2924)	23.4516	(18.6621,29.1061)
Peak unbalance	12.3789	(10.9116,13.7443)	35.1440	(25.9097,39.3678)
Kurtosis unbalance	1.9424	(1.119,2.508)	1.9406	(1.1183,2.5029)
MAV unbalance	6.6967	(3.2288,7.8592)	18.937	(9.1348,22.2252)
RMS free	9.8422	(6.8727,12.2968)	27.8328	(19.4356,34.2092)
Peak free	12.1378	(10.8709,13.7341)	34.8751	(30.4774,38.8487)
Kurtosis free	3.8453	(2.2105,5.3159)	3.679	(2.2089,3.8323)
MAV free	9.399	(3.5057,10.9723)	26.5808	(9.9178,31.0257)
RMS reference	1.1087	(0.70253,1.2483)	3.1351	(1.9865,3.53)
Peak reference	2.111	(2.0922,2.1314)	4.1658	(4.1422,4.1683)
Kurtosis reference	2.3455	(1.9455,3.8571)	3.341	(1.9445,3.8538)
MAV reference	0.8956	(0.3583,1.1323)	2.5328	(1.0138,3.2017)

The analysis continued with the RMS and kurtosis values. With the RMS values, the values of each sensor were separated into X and Y. To better observe the data, bar graphs were used, as shown in Figure 6, where we can see that the values in x will always be higher in their test (each pair of bars is a test). When reviewing these values, a boxplot graph is made comparing each sensor's values of sensor X with imbalance against the free X values, as shown in Figure 7. For the kurtosis values, the same separation of X and Y was performed, but only compared in the boxplots (Figure 8), which in the previous study showed more separation between them.

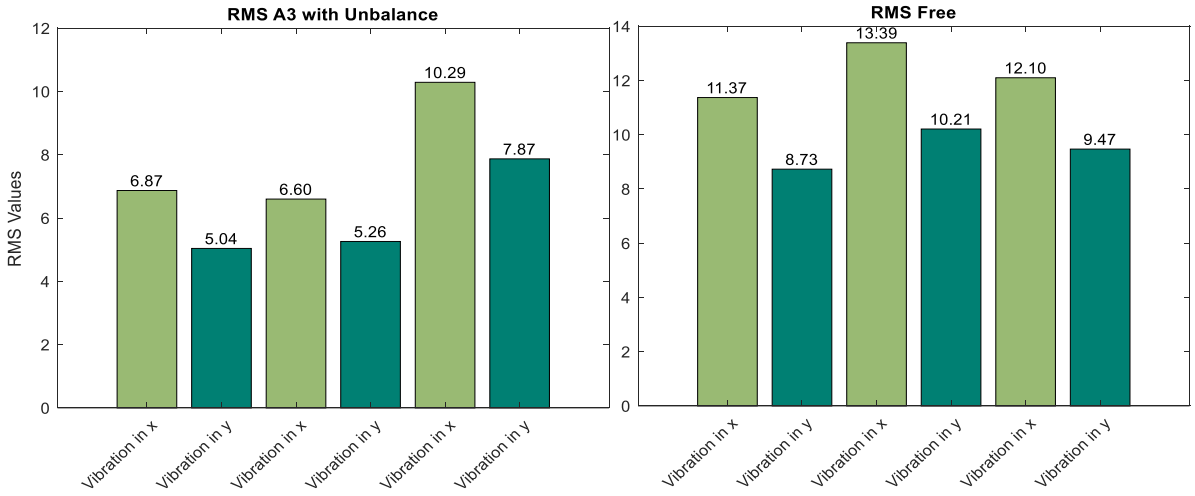

Figure 6. RMS values for each sensor in three different tests, complete decomposition

The RMS values in X with unbalance and free are observed to have a separation between them as seen in Figure 7 in the first two boxes, for Y with unbalance the same dynamics is observed this is observed in boxes 5 and 6, all this is also corroborated with the A3 data which is our last decomposition of the wavelet transform.

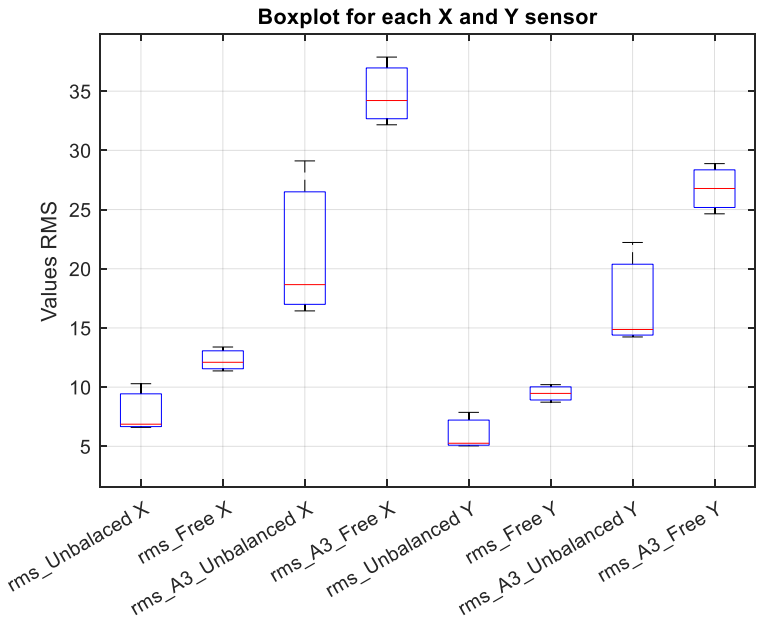

Figure 7. Boxplot Comparison of each sensor between the imbalance and free for RMS values

For the kurtosis values, Figure 8 shows a better separation for each of the pairs, and we see the data boxes with very uniform imbalance in both the X and Y axes.

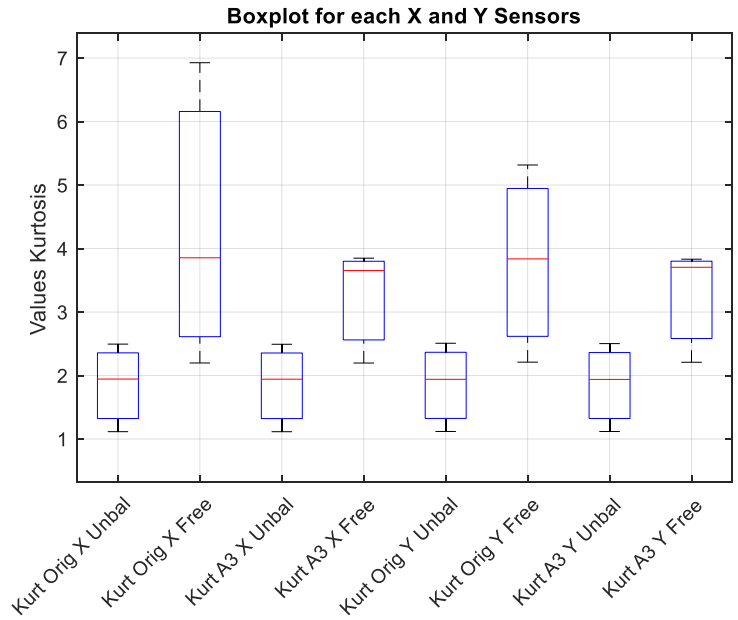

Figure 8. Boxplot comparison of each sensor between imbalance and free for kurtosis values

4. Conclusions

This study demonstrated that wavelet decomposition, particularly when analyzing the final approximation level cA3, allows for effective differentiation between balanced and unbalanced operating states in rotating machines (Figures 7 and 8). Among the characteristics analyzed, the RMS value and kurtosis showed a greater ability to distinguish between conditions, compared to the peak value and MAV, which showed minimal variability between the different scenarios. This suggests that RMS and kurtosis are more reliable indicators for detecting imbalance when using wavelet-based methods. Statistical evaluation using box plots and bar charts validated the ability of RMS values to distinguish between signals collected on the X and Y axes, both under normal and fault conditions, and more easily, the box plot for values using the kurtosis feature. The analysis of the cA3

level showed a significant contrast in the RMS and kurtosis distributions, reinforcing its diagnostic usefulness. In contrast, the first levels of decomposition generated values that were too similar to offer useful discrimination. Finally, the results obtained support the feasibility of implementing computationally efficient signal processing techniques for predictive maintenance tasks. It should be noted that even with low-complexity methods, such as RMS analysis based on wavelets, it is possible to obtain relevant information about the operating status of a machine. As future work, we propose to explore additional features and integrate machine learning techniques to improve the robustness of the classification and its generalization to different operating scenarios.

Declaration of competing interest

The authors declare that they have no known financial or non-financial competing interests in any material discussed in this paper.

Funding information

No funding was received from any financial organization to conduct this research.

References

[1] T. P. Carvalho, F. A. Soares, R. Vita, R. da P. Francisco, J. P. Basto, and S. G. S. Alcalá, "A systematic literature review of machine learning methods applied to predictive maintenance," *Comput. \& Ind. Eng.*, vol. 137, p. 106024, 2019.

[2] P. S. Ogun and M. R. Jackson, "Active vibration control and real-time cutter path modification in rotary wood planing," *Mechatronics*, vol. 46, pp. 21–31, 2017, doi: https://doi.org/10.1016/j.mechatronics.2017.06.007.

[3] S. Gawde, S. Patil, S. Kumar, P. Kamat, and K. Kotecha, "An explainable predictive maintenance strategy for multi-fault diagnosis of rotating machines using multi-sensor data fusion," *Decis. Anal. J.*, vol. 10, p. 100425, 2024, doi: https://doi.org/10.1016/j.dajour.2024.100425.

[4] A. Khadersab and S. Shivakumar, "Vibration Analysis Techniques for Rotating Machinery and its effect on Bearing Faults," *Procedia Manuf.*, vol. 20, pp. 247–252, 2018, doi: https://doi.org/10.1016/j.promfg.2018.02.036.

[5] L. D. Milfont, G. T. de Carvalho Ferreira, and M. Giesbrecht, "Fault diagnosis in electric machines and propellers for electrical propulsion aircraft: A review," *Eng. Appl. Artif. Intell.*, vol. 139, p. 109577, 2025, doi: https://doi.org/10.1016/j.engappai.2024.109577.

[6] P. Mallioris, E. Aivazidou, and D. Bechtsis, "Predictive maintenance in Industry 4.0: A systematic multi-sector mapping," *CIRP J. Manuf. Sci. Technol.*, vol. 50, pp. 80–103, 2024, doi: https://doi.org/10.1016/j.cirpj.2024.02.003.

[7] C. L. S. Rodriguez, E. A. Correa-Quintana, B. E. Tarazona-Romero, A. D. Rincón-Quintero, and J. G. Maradey-Lazaro, "Characterization of mechanical vibrations in a metal structure using the transform Cepstrum," *Period. Eng. Nat. Sci.*, vol. 9, no. 4, pp. 767–777, 2021.

[8] C. L. Sandoval-Rodriguez, J. G. Ascanio Villabona, C. G. Cárdenas-Arias, A. D. Rincon-Quintero, and B.

E. Tarazona-Romero, “Characterization of the mechanical vibration signals associated with unbalance and misalignment in rotating machines, using the cepstrum transformation and the principal component analysis,” *IOP Conf. Ser. Mater. Sci. Eng.*, vol. 844, no. 1, p. 12057, May 2020, doi: 10.1088/1757-899X/844/1/012057.

[9] W. Jiang, J. Wu, Y. Yang, X. Li, and H. Zhu, “Health evaluation techniques towards rotating machinery: A systematic literature review and implementation guideline,” *Reliab. Eng. Syst. Saf.*, vol. 260, p. 110924, 2025, doi: https://doi.org/10.1016/j.ress.2025.110924.

[10] Y. Feng *et al.*, “Beyond deep features: Fast random wavelet kernel convolution for weak-fault feature extraction of rotating machinery,” *Mech. Syst. Signal Process.*, vol. 224, p. 112057, 2025, doi: https://doi.org/10.1016/j.ymssp.2024.112057.

[11] C. Cárdenas, C. Sandoval, A. Rincón, D. Galván, and H. Téllez, “Data Collector Design for Vibration Analysis by Raspberry pi 3B Embedded System Means for Industrial Applications,” *J. Phys. Conf. Ser.*, vol. 2224, no. 1, p. 12032, Apr. 2022, doi: 10.1088/1742-6596/2224/1/012032.

[12] C. L. Sandoval-Rodríguez, C. L. Higuera, J. G. Ascanio-Villabona, A. D. Rincón Quintero, and J. G. Maradey-Lazaro, “Flow Control Strategies Using Classical Regulatory Technique and Advanced H2 Technique in an Irrigation Emulation Pilot Plant,” in *Recent Advances in Electrical Engineering, Electronics and Energy*, M. Botto-Tobar, H. Cruz, and A. Díaz Cadena, Eds., Cham: Springer International Publishing, 2022, pp. 56–72.

[13] A. Ainapure, X. Li, J. Singh, Q. Yang, and J. Lee, “Enhancing Intelligent Cross-Domain Fault Diagnosis Performance on Rotating Machines with Noisy Health Labels,” *Procedia Manuf.*, vol. 48, pp. 940–946, 2020, doi: https://doi.org/10.1016/j.promfg.2020.05.133.

[14] S. Bertagna, L. Braidotti, V. Bucci, and A. Marinò, “An innovative methodology for enabling predictive maintenance of ship systems based on Industry 4.0 technologies,” *Procedia Comput. Sci.*, vol. 253, pp. 2389–2398, 2025, doi: https://doi.org/10.1016/j.procs.2025.01.299.

[15] M. Vishwakarma, R. Purohit, V. Harshlata, and P. Rajput, “Vibration Analysis & Condition Monitoring for Rotating Machines: A Review,” *Mater. Today Proc.*, vol. 4, no. 2, Part A, pp. 2659–2664, 2017, doi: https://doi.org/10.1016/j.matpr.2017.02.140.

[16] J. R. A. Montoya, “La transformada wavelet,” *Rev. la Univ. Mendoza*, 2001.

[17] E. P. Serrano, M. Fabio, and A. Figliola, “Time-frequency methods based on the wavelet transform,” 2012.

[18] J. Colin Ocampo, J. G. Mendoza Larios, A. Blanco Ortega, A. Abúndez Pliego, and E. S. Gutiérrez Wing, “Determinación del Desbalance en Sistemas Rotor-cojinete a velocidad constante: Método de Identificación Algebraica,” *Ing. mecánica, Tecnol. y Desarro.*, vol. 5, no. 4, pp. 385–394, 2016.

[19] U. Ates and H. Copur, “Investigation into vibration patterns generated by full-scale linear rock cutting tests,” *Tunn. Undergr. Sp. Technol.*, vol. 162, p. 106635, 2025, doi:

https://doi.org/10.1016/j.tust.2025.106635.

[20] J. Igba, K. Alemzadeh, C. Durugbo, and E. T. Eiriksson, “Analysing RMS and peak values of vibration signals for condition monitoring of wind turbine gearboxes,” *Renew. Energy*, vol. 91, pp. 90–106, 2016, doi: https://doi.org/10.1016/j.renene.2016.01.006.

[21] M. Elsamanty, A. Ibrahim, and W. S. Salman, “Principal component analysis approach for detecting faults in rotary machines based on vibrational and electrical fused data,” *Mech. Syst. Signal Process.*, vol. 200, p. 110559, 2023.

[22] A. Baldini, R. Felicetti, F. Ferracuti, A. Freddi, S. Iarlori, and A. Monteriù, “Real-time propeller fault detection for multirotor drones based on vibration data analysis,” *Eng. Appl. Artif. Intell.*, vol. 123, p. 106343, 2023, doi: https://doi.org/10.1016/j.engappai.2023.106343.